Molecular Physics, Vol. 104, No. 8, 20 April 2006, 1217–1225

Taylor & Francis
Taylor & Francis Group

Intermolecular hyperfine tensor for Xe@O_2. Density and temperature dependence of Xe chemical shifts in oxygen gas

L. VUKOVIC†, C. J. JAMESON*† and D. N. SEARS‡
†University of Illinois at Chicago, USA
‡University of Alberta, Edmonton, Canada

(*Received 7 July 2005; in final form 25 August 2005*)

For the first time, the intermolecular hyperfine tensor at a ^{129}Xe nucleus close to an O_2 molecule has been calculated for various configurations. The quality of this quantum mechanical calculation has been tested against the experimentally measured density and temperature-dependent chemical shifts of ^{129}Xe in the limit of zero mole fraction of Xe in O_2 gas.

1. Introduction

Xe has been demonstrated to be an ultra-sensitive probe of the electronic structure, and the configurational structure and dynamics of its environment [1–3]. The very large ^{129}Xe NMR chemical shifts that arise when the Xe atom finds itself inside the pores and channels of zeolites, polymers, biomolecules, or on the surface of metals or metal clusters, permit discrimination between environments according to the types of atoms and the dynamics of the atoms that constitute the inside of the pore or channel [4], the dimensions of the cages or channels [5], the symmetry of the cages [6], the aspect ratio of the cross-sections of channels [4], the exchange dynamics of Xe atoms within the porous materials [7, 8], and even such subtle differences as degree of deuterium substitution of cages that trap the Xe atom [9]. The very large range of intermolecular chemical shifts for Xe atom in these various environments, which makes such discriminations possible, arises from the fact that interactions with the electrons of the Xe atom amplify the shielding response at the ^{129}Xe nucleus from a neighbouring molecule in diamagnetic systems.

When placed in an external magnetic field, the unpaired electron spins of the paramagnetic centres within the sample provide an additional local field at the position of each neighbouring nucleus. The magnitude of this local field will determine the additional shift of the ^{129}Xe NMR signal beyond that of the diamagnetic system. We expect that the electrons of Xe atom will amplify molecular spin densities at the ^{129}Xe nucleus, thus giving rise to large hyperfine shifts of the Xe nucleus that can provide the basis for the application of ^{129}Xe NMR as an ultra-sensitive probe for the detection of the presence and the distribution of paramagnetic centres in the sample. There are experimental reports of large unusual ^{129}Xe chemical shifts in porous materials where paramagnetic centres may be present [10], but the results were largely unexplained in part because of lack of model systems for comparison and the lack of independent structural information. More recently, a large change in the line shape and in the isotropic value of the ^{129}Xe chemical shift was observed for Xe in the hexagonal channels of a molecular crystal of $Co(en)_3Cl_3$ upon replacing the Co^{3+} ion with a Cr^{3+} ion [11]. Towards an understanding of the Xe response to paramagnetic centres in porous materials, in this paper, we consider a simple system, Xe@O_2, in which experimental data is available in the gas phase where a straightforward connection between theoretical calculations and experiment exists.

Xe atoms in oxygen gas exhibited large downfield shifts that were of the same direction but about one order of magnitude larger per solvent molecule number density than had been reported for other gases at room temperature [12]. Buckingham and Kollman found that using only the overlap mechanism, in particular the overlap between a 5s orbital on the Xe atom and the π_g^* molecular orbital of the O_2 molecule, was sufficient to produce a paramagnetic shift of approximately the right order of magnitude at the ^{129}Xe nucleus [13]. The temperature dependence of the density coefficient was subsequently examined and the number density coefficient of the chemical shift was found to exhibit

*Corresponding author. Email: cjjames@uic.edu

Molecular Physics
ISSN 0026–8976 print/ISSN 1362–3028 online © 2006 Taylor & Francis
http://www.tandf.co.uk/journals
DOI: 10.1080/00268970500525614

a $1/T$ dependence at low temperatures (below 350 K) where the contributions from the Fermi contact interaction, which is expected to show this Curie-type behaviour, dominates over the normal ^{129}Xe chemical shifts from interaction with diamagnetic molecules [14]. Although the temperature behaviour at low temperatures provides the signature that definitively identifies a mechanism for at least a part of the large paramagnetic shifts, a quantitative first principles interpretation has been lacking up till now.

In this paper, we carry out quantum mechanical calculations of the hyperfine tensor at the ^{129}Xe nucleus and express this hyperfine tensor as a mathematical surface, a general function of distance and angle in the configuration of the Xe@O_2 van der Waals molecule. We also calculate the ^{129}Xe nuclear shielding tensor at the same configurations. We previously conducted tests of the ^{129}Xe nuclear shielding surface for similar systems of diamagnetic molecules (CO, N_2, CO_2) and we expect the Xe@O_2 nuclear shielding tensor to be of comparable quality. We test the quality of the hyperfine tensor surface by calculating the temperature dependence of the total density coefficient of the ^{129}Xe chemical shift arising from the combination of the usual intermolecular mechanism in diamagnetic systems and the hyperfine tensor mechanism and comparing this with that observed experimentally [14].

For the density and temperature dependence of the ^{129}Xe chemical shift in O_2 gas, only the isotropic part of the hyperfine tensor, the Fermi contact part, can contribute since the traceless dipolar part averages isotropically to zero in the gas phase. On the other hand, the traceless dipolar part is responsible for the electron spin dipole nuclear spin dipole mechanism for the relaxation of ^{129}Xe nuclear spin in the gas phase mixtures containing O_2, which we have measured in this laboratory [15]. A comment on this experimental consequence of the hyperfine tensor at the ^{129}Xe nucleus is given below.

2. Methods and results

2.1. *The Xe@O_2 potential function*

The anisotropic potential energy of interaction between Xe atom and O_2 molecule for intermediate and large intermolecular distances has been formulated by Aquilanti *et al.* [16] based on two experimental components in which the total integral cross-sections for scattering are measured in the thermal energy range as a function of the collision energy and under a controlled alignment of the rotational angular momentum: (a) Data obtained with a hot effusive molecular beam probe the spherical component of the potential energy surface. (b) Data from supersonic seeded beams, where the oxygen molecules are cooled at the $K=1$ rotational level, and selectively aligned probe the anisotropy of the potential surface. Analysis of the experimental results were carried out by Aquilanti *et al.* using close coupling exact quantum mechanical calculations of the cross sections. The resulting potential function is of the form [16]

$$V(R,\theta) = V_0(R) + V_2(R)P_2(\cos\theta) + V_4(R)P_4(\cos\theta) \quad (1)$$

where $P_n(\cos\theta)$ are Legendre polynomials. $V_0(R)$ represents the spherical component of the interaction in a Morse–spline–van der Waals parametrization as follows. The scaled distance and energy are

$$x = R/R_m, \quad f(x) = V_0(R)/\varepsilon \quad (2)$$

Morse,

$$f(x) = \exp[-2\beta(x-1)] - 2\exp[-\beta(x-1)], \quad \text{for } x \le x_1 \quad (3)$$

spline,

$$f(x) = b_1 + b_2(x-x_1) + [b_3 + b_4(x-x_1)](x-x_2), \quad \text{for } x_1 < x < x_2 \quad (4)$$

van der Waals,

$$f(x) = -(C_0/\varepsilon R_m^6)x^{-6}, \quad \text{for } x \ge x_2(3) \quad (5)$$

The interaction anisotropy is given by the coefficients of the $P_n(\cos\theta)$ terms:

$$V_2(R) = A_2\exp(-\alpha R) - a_2 C_0 R^{-6} \quad (6)$$

$$V_4(R) = A_4\exp(-\alpha R) \quad (7)$$

Parameters of the Aquilanti potential are given in [16]. The global minimum of the Xe@O_2 system is at (0.387 nm, 90°) with a well depth of 207 K. The collinear configuration has a minimum farther out at (0.430 nm, 0°) with a well depth of 150 K.

2.2. *The Xe@O_2 shielding and spin density as functions of configuration*

For the Xe atom, we used an uncontracted 29s 21p 17d 9f set, 240 basis functions in all, that we have

found to provide an accurate ^{129}Xe shielding response at various orientations and intermolecular separations in other xenon van der Waals complexes. The core (26s19p13d) was taken from Partridge and Faegri [17]; this was augmented by 3s, 2p, 4d, and 9f orbitals with exponents taken from D. Bishop [18]. For O atoms we used a Huzinaga 11s7p basis set [19] augmented with three d functions [17]. Calculations were carried out in Gaussian98 [20], using gauge-including atomic orbitals (GIAO) [21] in density functional theory with the B3LYP hybrid functional.

Calculated Xe shielding values $\sigma(R,\theta)$ for Xe@O_2 at 70 (R,θ) points were expressed in the following functional form:

$$\{\sigma(R,\theta)-\sigma(\infty)\}=\sum_{p=6,\,\text{even}}^{12}R^{-p}\sum_{\lambda=0,\,\text{even}}^{6}a_{p\lambda}P_\lambda(\cos\theta), \quad (8)$$

where P_λ is a Legendre polynomial and the coefficients $a_{p\lambda}$ were obtained by a non-linear least squares fitting procedure. An essential constraint that must be imposed on the fitting function is that the long-range behaviour of the intermolecular shielding be correct. The calculated points remain negative (deshielded) as R approaches large distances, up to 6 Å. The fitting was therefore constrained to keep the values of the function less than zero at 12 points: at 4, 5, 6, and 7 Å, at $\theta=0°$, 45°, and 90°. This surface, shown in figure 1 is found to be very similar to the Xe@N_2 shielding surface, typical of shielding surfaces for Xe interacting with small linear molecules, with the Xe@O_2 exhibiting somewhat smaller magnitudes at the same (R,θ) compared to Xe@N_2.

Calculated net electron spin densities at the Xe nucleus $\rho(R,\theta)$ at 70 (R,θ) points were expressed in the following functional form:

$$\{\rho(R,\theta)-\rho(\infty)\}=\sum_{p=6,\,\text{even}}^{12}R^{-p}\sum_{\lambda=0,\,\text{even}}^{6}b_{p\lambda}P_\lambda(\cos\theta), \quad (9)$$

where P_λ is a Legendre polynomial and the coefficients $b_{p\lambda}$ were obtained by a similar least squares fitting procedure as for the shielding, with analogous constraints. This spin density surface is shown as the actual calculated points at various configurations in figure 2.

Compared with figure 1, the spin density surface is quite unlike the typical shielding surfaces for Xe interacting with N_2, O_2, or CO_2 in that it exhibits extrema at $\theta=45°$ and 90°. This angle dependence is easily explained. In the free O_2 molecule,

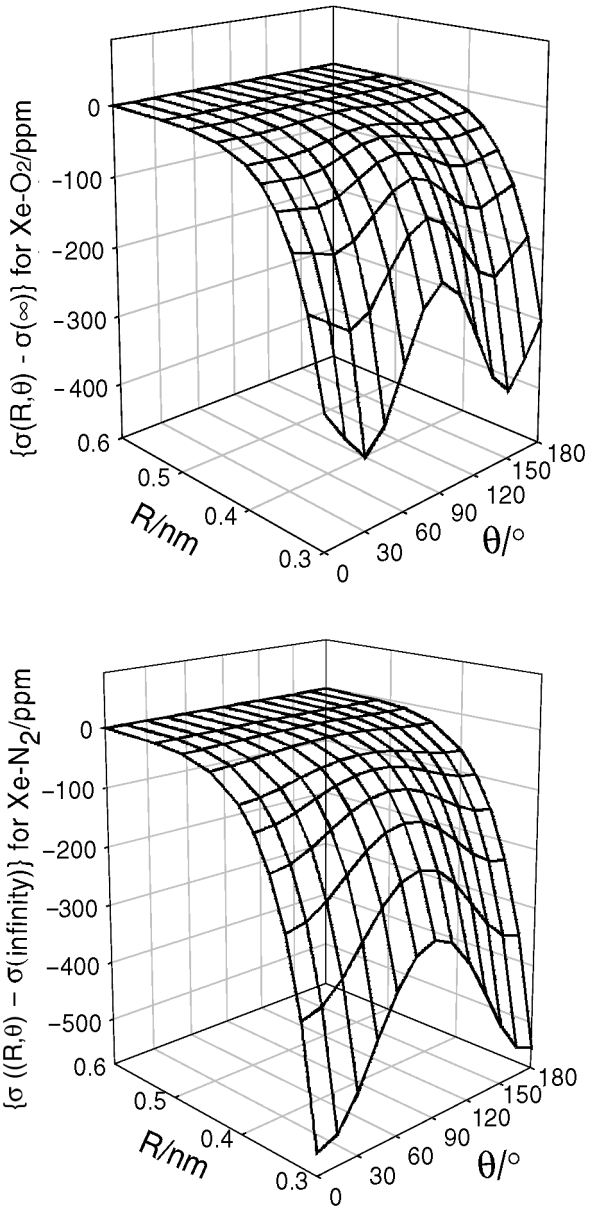

Figure 1. Quantum mechanical values of the intermolecular Xe shielding (relative to the free Xe atom) as a function of Xe@O_2 configuration (top), compared with that of Xe@N_2 (bottom).

the contribution to the spin density comes largely from the antibonding π_g^* molecular orbitals which have nodal planes passing through the center of the molecule and normal to the bond axis. The Xe atom approaching along $\theta=90°$ lies on this nodal plane, thus exhibits no response to the spin density of the O_2 molecule. The greatest spin density in π_g^* of the free O_2 molecule is encountered by Xe along the $\theta=45°$ approach.

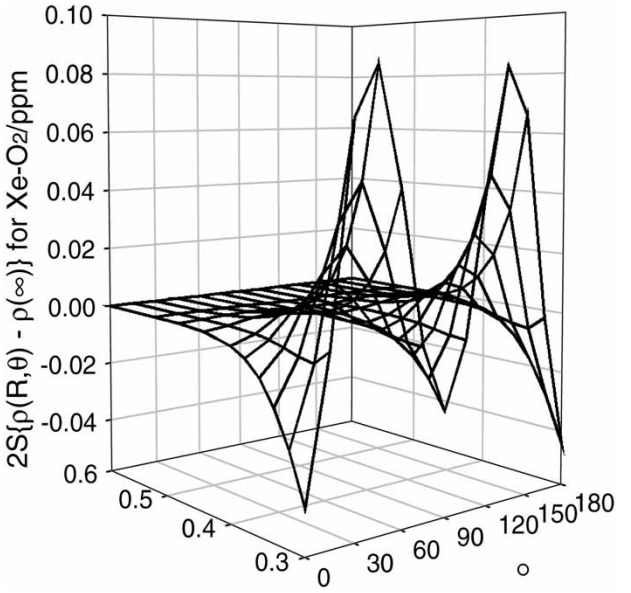

Figure 2. Quantum mechanical values of the isotropic Fermi contact portion of the hyperfine tensor, expressed as net spin densities at the Xe nucleus as a function of Xe@O_2 configuration.

3. Comparison with experiment

The interaction term $\boldsymbol{A}_{\mathrm{Xe}} \bullet \boldsymbol{I}$ in the spin Hamiltonian of the Xe@O_2 complex leads to a local magnetic field at the Xe nucleus:

$$\langle \Delta B/B_0 \rangle = (1/\hbar \gamma_{\mathrm{Xe}} B_0) \langle \boldsymbol{A}_{\mathrm{Xe}} \rangle \bullet \hat{k} \tag{10}$$

where the average over thermally populated states is indicated by $\langle\,\rangle$, and where the static magnetic field, B_0, has a fixed orientation $\hat{k}$ with respect to the axis system of the complex. Here, the Fermi contact part $\boldsymbol{A}_{\mathrm{Xe,\ Fermi}} \bullet \boldsymbol{I}$ is given by:

$$\boldsymbol{A}_{\mathrm{Xe,\,Fermi}} \bullet \boldsymbol{I} = (16\pi/3)\hbar\ \mu_{\mathrm{B}} \gamma_{\mathrm{Xe}} \sum_i \delta(r_i) s_i I \tag{11}$$

in which the sum is over the electrons i, s_{i} is the spin operator and $\boldsymbol{r}_i$ is the vector from the ith electron to the Xe nucleus. And the traceless dipolar part $\boldsymbol{A}_{\mathrm{Xe,\,dipolar}} \bullet \boldsymbol{I}$ is given by:

$$\boldsymbol{A}_{\mathrm{Xe,\,dipolar}} \bullet \boldsymbol{I} = 2\hbar \mu_{\mathrm{B}} \gamma_{\mathrm{Xe}} \sum_i \left\{ \frac{3(r_i \bullet s_i)(r_i \bullet I)}{r_i^5} - \frac{s_i \bullet I}{r_i^3} \right\} \tag{12}$$

The vector position $\boldsymbol{r}_i$ is in the x,y,z molecule-fixed axis system, and in general, of course, the B_0 direction

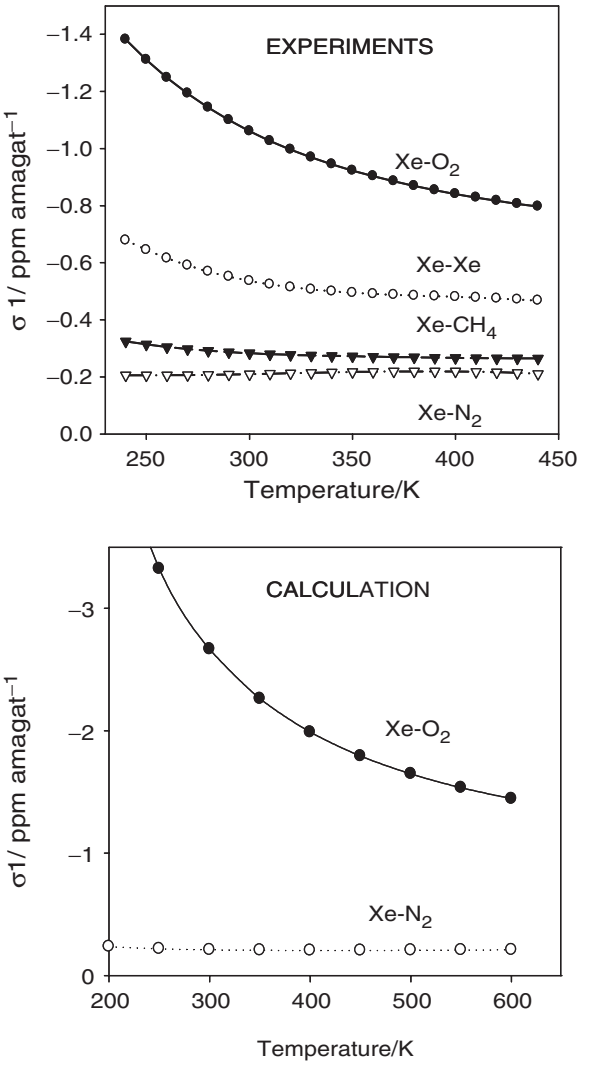

Figure 3. Comparison of the total density coefficient of the Xe chemical shifts, $\sigma_1(\mathrm{T})/\mathrm{ppm\ amagat}(O_2)^{-1}$ for Xe in O_2 gas calculated in this work against experimental values of previous work.

$\hat{k}$ does not lie along the z axis. In the system, we are considering, there is no $\boldsymbol{A}_{\mathrm{Xe,\,orbital}} \bullet \boldsymbol{I}$ contribution.

At any instantaneous orientation, the average over thermally populated states is given by [22]:

$$\left(\frac{\Delta B}{B_0}\right) = \left(\hbar \gamma_{\mathrm{Xe}} B_0 kT \sum_n e^{-E_n/kT}\right)^{-1}$$

$$\times \left\{ \begin{array}{l} \sum\limits_{n,m} \left(e^{-E_n/kT}\right) \times \langle n|\mu_e \bullet B_0|m\rangle \langle m|A_{\mathrm{Xe}} \bullet \hat{k}|n\rangle \\ \\ -kT \sum\limits_{n,m \neq n} \left(\dfrac{e^{-E_n/kT} - e^{-E_m/kT}}{E_n - E_m}\right) \times \langle n|\mu_e \bullet B_0|m\rangle \langle m|A_{\mathrm{Xe}} \bullet \hat{k}|n\rangle \end{array} \right\} \tag{13}$$

for pure $\boldsymbol{S}$ (no $\boldsymbol{L}$), $\boldsymbol{\mu}_e = -g\ \mu_B\ \boldsymbol{S}$, $\mu_B = e\eta/2mc$ is the Bohr magneton. The $|n\rangle$ and $|m\rangle$ are the eigenfunctions of the field-independent Hamiltonian, which are superposition of states $|\alpha S_z\rangle$ which depend on quantum numbers, of which one is the eigenvalue of S_z and the other quantum numbers are represented by α. For Xe@O_2, n and m are the various components of the triplet manifold. For comparison, the accessible electronic eigenstates for the NO molecule are the $\Pi_{1/2}$ and the $\Pi_{3/2}$ states.

For molecules tumbling freely in the gas phase, and for very short T_{1e} (electron spin–lattice relaxation time), thermal equilibrium among the thermally populated states is established rapidly relative to any motion of the molecule. If the reciprocal of the rotational correlation time of the complex is much less than the anisotropy $E_{max}-E_{min}$ of the E_n-E_m in the above equation in frequency units, equation (13) is valid for any instantaneous orientation. Therefore, for complexes in which these conditions are satisfied, the isotropic chemical shift in the gas phase is obtained by simply averaging equation (13) over all orientations of the molecular complex in the laboratory frame of B_0. However, for the Xe atom in O_2 gas, there is additionally, the whole family of nuclear configurations (R,θ) that is sampled over, with the probability of each configuration being determined by $\exp[-V(R,\theta)]/kT$, with R from 0 to ∞ and $\theta = 0$ to π, and with the $\boldsymbol{A}_{Xe}$ itself being a function of nuclear configurations (R,θ) and including only $\boldsymbol{A}_{Xe} = (16\pi/3)\hbar\mu_B\gamma_{Xe}\ \sum_i \delta(r_i)s_i$, since in this case the traceless dipolar term shown in equation (12) averages to zero. Thus, we have for the Xe atom in O_2 gas,

$$\left(\frac{\Delta B}{B_0}\right)_{R,\theta} = 16\pi\mu_B\left(9kT\sum_n e^{-E_n/kT}\right)^{-1} \times \sum_{\alpha=x,y,z}\left\{\begin{array}{l}\sum_{n,m}\left(e^{-E_n/kT}\right)\times\langle n|\mu_\alpha|m\rangle\langle m|\sum_i \delta(r_i)s_{i\alpha}|n\rangle \\ -kT\sum_{n,m\neq n}\left(\dfrac{e^{-E_n/kT}-e^{-E_m/kT}}{E_n-E_m}\right)\times\langle n|\mu_\alpha|m\rangle\langle m|\sum_i \delta(r_i)s_{i\alpha}|n\rangle\end{array}\right\}_{R,\theta} \tag{14}$$

Neglecting the zero field splitting, this reduces to

$$\left(\frac{\Delta B}{B_0}\right)_{R,\theta} = -[8\pi S(S+1)g_e^2\mu_B^2/9kT]\{\rho(R,\theta)-\rho(\infty)\} \tag{15}$$

where, $S(S+1)=2$ for the Xe@O_2 system. The sign of the electron spin density at the Xe nucleus, $\{\rho(R,\theta)-\rho(\infty)\}$, is negative when the probability density of the β spin dominates over the α at Xe nuclear position (R,θ). The quantity $\{\rho(R,\theta)-\rho(\infty)\}$ is evaluated at each particular configuration (R,θ) and the averaging over all configurations is carried out by

$$\sigma_1(T)_{hyperfine} = \left(\frac{\Delta B}{B_0}\right)_{thermal\_average}(T) = -(16\pi g_e^2\mu_B^2/9kT)\bullet 2\pi\int_{\theta=0}^{\pi}\int_{R=0}^{\infty}\{\rho(R,\theta)-\rho(\infty)\} \times \exp^{-V(R,\theta)/kT} r^2 dr\sin\theta d\theta \tag{16}$$

The other contribution to the density coefficient of the Xe chemical shift is obtained by

$$\sigma_1(T)_{diamagnetic} = 2\pi\int_{\theta=0}^{\pi}\int_{R=0}^{\infty}\{\sigma(R,\theta)-\sigma(\infty)\} \times \exp^{-V(R,\theta)/kT} r^2 dr\sin\theta d\theta \tag{17}$$

where the $\{\sigma(R,\theta)-\sigma(\infty)\}$ is obtained from the fitted quantum mechanical values expressed in the functional form given in equation (8). The molar paramagnetic bulk susceptibility χ of oxygen provides a sample-shape-specific contribution which is

$$\sigma_1(T)_{bulk} = (2\pi/3)\chi = +0.3093\ (300/T)\text{ppm amagat}^{-1}, \tag{18}$$

under the conditions of the experiment, that is with a cylindrical sample having its axis oriented perpendicular to the magnetic field direction [14]. The resulting sum of values from equations (16), (17) and (18) at each temperature can be compared with the experimental values of $\sigma_1(T)$ given in figure 1 of [14] and described by the empirical function given therein for the temperature range 260–440 K:

$$\sigma_1(T)_{Xe-O_2}\ \text{ppm amagat}^{-1} = -1.0610 + 3.64\times10^{-3}(T-300) - 2.187\times10^{-5}(T-300)^2 + 9.583\times10^{-8}(T-300)^3 - 2.075\times10^{-10}(T-300)^4 \tag{19}$$

where, one amagat is the number density of an ideal gas at standard conditions of temperature and pressure. The comparison between the calculated and experimental values is shown in figure 3, where we find only semi-quantitative agreement with experimental values.

Hartree–Fock results for shielding are found to be missing about 15% in tests against experiments in rare-gas mixtures [23]. We had previously attributed the entire difference between experiment and Hartree–Fock

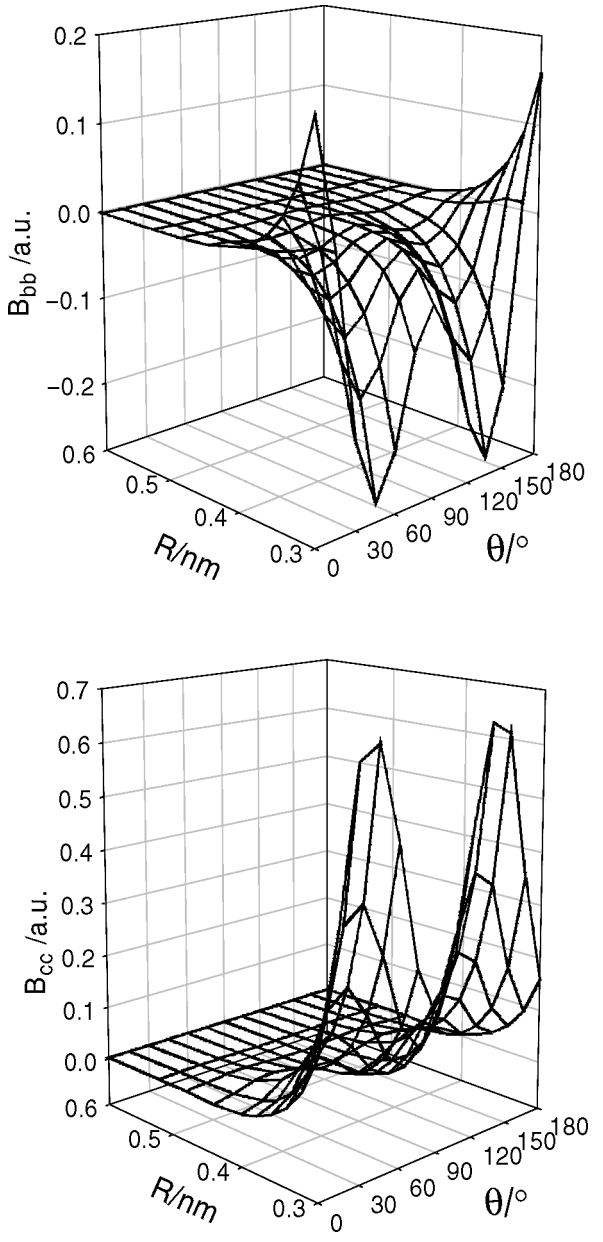

Figure 4. Quantum mechanical values of two principal components of the traceless dipolar part of the hyperfine tensor at the Xe nucleus, as a function of Xe@O_2 configuration.

results as entirely due to electron correlation, which DFT-B3LYP appears to overestimate by about 15% [23, 24]. On the other hand DFT-B3LYP here appears to overestimate the Fermi contact term for ^{129}Xe in O_2 by about a factor of 3. We are using the same level of theory and the same 240 basis functions on Xe atom. So why are the results for the Fermi contact term so much worse compared to experiment? All calculations we have done are non-relativistic calculations. It is known that the diamagnetic shielding of the free Xe atom calculated using relativistic methods is much larger than that obtained using any non-relativistic method [25]. In comparing Hartree–Fock results for ^{129}Xe against experiments, we have attributed the entire difference to electron correlation, under the assumption that the free Xe atom shielding and the shielding of the Xe atom in the presence of the neighbour atom contain the same relativistic effects, and that there is little relativistic contribution to the interaction part of the shielding. This appeared to be a reasonable assumption, given that most of the difference between the non-relativistic and the relativistic results for the free Xe atom come from the contributions of the 1*s* electrons, which are hardly involved in the intermolecular shielding response. It is interesting to note that electron correlation and relativistic corrections to the electric field effects on the shielding of the Xe atom have been found recently to be opposite in sign [26]. Therefore, although the relativistic calculations have not yet been carried out for Xe-rare gas systems, the electron correlation contributions and relativistic corrections to the intermolecular shielding in Xe-rare gas or other Xe-neighbours, are, like the shielding polarizability of the Xe atom, likely to be opposite in sign. The electron correlation contributions to the intermolecular shielding of Xe atom have recently been calculated at the CCSD level [27], and for Xe-rare gas the results are not much different from those obtained using DFT-B3LYP [23]. Thus, it is likely that part of the 15% overestimate of the interaction shielding response by DFT-B3LYP in [23] comes from neglect of relativistic effects. At the same time the entire 15% difference between Hartree–Fock results and experiments must be due to both electron correlation and relativistic effects. On the basis of comparisons with experimental gas phase second virial coefficients, relativistic effects on intermolecular shielding is of the order of the discrepancy between the best correlated non-relativistic calculations and experiment, that is, of the order of only a few per cent [27].

In qualitative terms, one of the known consequences of relativistic behaviour of electrons in an atom is the contraction of the *s* and *p* orbitals, and this effect is very pronounced in the lanthanide series, leading to much smaller atomic diameters and much shorter equilibrium bond lengths than resulting from non-relativistic treatments. Let us consider the two interaction response properties at the ^{129}Xe nucleus. The shielding response is largely due to contributions from the non-zero angular momentum orbitals (p, d, f) by the very nature of the operators that are involved in that part of the shielding that dominates the interaction shielding response. Contraction of the *p* orbitals is not reflected

in non-relativistic description, leading to overestimated results for their contributions to the interaction shielding response. At the same internuclear distance, more realistic contracted orbitals should provide a smaller interaction shielding response. Thus, electron correlation and relativistic corrections will be opposite in sign.

Why is the Fermi contact portion of the hyperfine tensor of Xe@O_2 so greatly overestimated by DFT-B3LYP? There is an important difference between the interaction shielding response and the transferred hyperfine response at Xe. Looking at the latter from a mechanistic point of view, the net spin density at the Xe nucleus arises from (a) the net spin density from the O_2 molecule at the position of the Xe nucleus, which would be present in the absence of the electrons of the Xe atom, (b) the transferred spin polarization arising from the interactions between the electrons in the π_g^* orbitals of O_2 and the electrons in the *s* orbitals of Xe atom which have density at the Xe nucleus, and (c) the transferred spin polarization arising from the interactions between the electrons in the π_g^* orbitals of O_2 and the electrons in the *p*, *d*, *f* orbitals of Xe atom, which, in turn, transfer their polarization to the *s* orbitals, including the inner ones such as 1*s*.

Contracted *p* orbitals will provide less interaction shielding response and also less polarization transfer from π_g^* orbitals of O_2, so non-relativistic calculations of both the shielding response and the Fermi contact transferred hyperfine have this same difficulty, with errors in the same direction of overestimation by non-relativistic calculations. On the other hand, the Fermi contact transferred hyperfine has the additional factor that the error is amplified by much higher density of contracted *s* orbitals, particularly the inner ones, at the nucleus in relativistic atoms, as shown historically by relativistic calculations of another NMR observable, the electron-mediated internuclear spin–spin coupling [28–32]. While non-relativistic DFT-B3LYP gives only small errors ($<15\%$) in the calculated shielding response for Xe atoms in the presence of neighbouring diamagnetic neighbours, it gives much larger errors (overestimates by a factor of 3) for the calculated transferred hyperfine for ^{129}Xe in the presence of neighbouring paramagnetic neighbor O_2. Relativistic calculations of the hyperfine tensor in the Xe@O_2 system are needed.

4. Comments on the ^{129}Xe spin relaxation in the presence of O_2

Nuclear spin relaxation by intermolecular dipolar interaction has been considered in a formal kinetic theory and also in a correlation function approach. Chen and Snider used a quantum mechanical formulation of molecular kinetic theory (Waldman–Snider), and they related the observed relaxation time T_1 to scattering matrices which describe the rotationally inelastic and elastic molecular collisions [33]. In the so-called extreme narrowing limit, both approaches lead to expressions for the intermolecular dipolar relaxation of spin *I* by spin *S* (^{129}Xe and O_2, respectively) which can be written in the form [15]

$$\frac{1}{T_1}=\frac{16}{3}S(S+1)\gamma_I^2\gamma_S^2\frac{\hbar^2}{d^2}\left(\frac{\pi\mu}{8kT}\right)^{1/2}N_S F(V/kT)\{1-f(T)\omega_I^{1/2}\} \tag{20}$$

where N_S is the number density of *S*-bearing molecules. γ_I and γ_S are the magnetogyric parameters of the spins *I* and *S*, and *d* is the characteristic length of the intermolecular interaction, loosely referred to as the molecular diameter. The $(\pi\mu/8kT)^{1/2}$ term is the reciprocal mean relative velocity. The factor $F(V/kT)$ can be written in terms of a general anisotropic intermolecular potential, and it has been shown that this factor could be viewed as a collision efficiency for relaxation [15]. The magnetic field dependence in $f(T)\omega_I^{1/2}$ was arrived at using a correlation function approach [15]. Collision theory calculations of intermolecular dipole–dipole relaxation rates in the gas phase involve nuclear spin point dipoles sited on the collision partners of the molecule bearing the relaxing nucleus; one needs the anisotropic intermolecular potential function. The intermolecular dipole–dipole relaxation involving unpaired electron spins cannot be described in the same way, because the electron spin density is delocalized over the entire Xe@O_2 collision complex. In the latter system, the nuclear spin dipole–electron spin dipole interaction is described in terms of the dipolar part of the hyperfine tensor of the complex at the ^{129}Xe nucleus.

We have obtained the full hyperfine tensor in the quantum mechanical calculations. Two components of the traceless dipolar part of the tensor are shown as a function of *R* and θ in figure 4.

The factor $F(V/kT)$ in the relaxation rate expression will depend on both the anisotropic Xe–O_2 potential function and the dipolar part of the hyperfine tensor as a function of configuration. Thus, the components of the dipolar part of the hyperfine tensor, each one a mathematical surface in (R,θ), can be used to provide a theoretical calculation of the intermolecular dipole–dipole relaxation contribution to the spin–lattice relaxation rate of the ^{129}Xe nucleus, which has been previously characterized experimentally in our

laboratory in terms of dependence on number density, temperature, and ω_I (applied magnetic field) [15]. Spin relaxation rates are known to be stringent tests of the quality of intermolecular potentials [34].

5. Conclusions

We have calculated for the first time, the intermolecular hyperfine tensor at a Xe nucleus close to an O_2 molecule for various configurations. The quality of the non-relativistic quantum mechanical calculation has been tested against the experimentally measured density and temperature-dependent chemical shifts of Xe in the limit of zero mole fraction of Xe in O_2 gas. The results of this test of the isotropic part of the hyperfine tensor are encouraging, but are only in semi-quantitative agreement with experiment. We propose that relativistic calculations can bring the results closer to experiment. We find it reasonable that the relativistic effects on the Fermi contact part of the hyperfine tensor are a larger fraction of the observed shifts due to paramagnetic centres, than the relativistic effects on the intermolecular shifts that are due to diamagnetic neighbour molecules. The dipolar part of the hyperfine tensor is yet to be tested against the spin lattice relaxation times measured for Xe in mixtures of xenon and O_2 gas as a function of density and temperature.

We have shown that the Fermi contribution leads to an apparent chemical shift that is sensitive to the distance and the orientation of the paramagnetic centre relative to Xe. We propose that the chemical shift of a Xe atom confined to a channel or cavity in a porous material can provide information about positions and orientations of paramagnetic centres. In a separate study, we are using the results of quantum mechanical calculations of Xe hyperfine tensors, of the type carried out in the present work, as models for the interpretation of Xe line shapes in confined geometries in materials doped with paramagnetic molecules or ions. The Fermi contribution can have dramatic effects on the average Xe chemical shift, while the dipolar contribution can influence the apparent average Xe chemical shift tensor components evident in the singularities of the Xe NMR line shape.

Acknowledgements

This research was supported by the National Science Foundation (Grant CHE–9979259). DNS thanks the Alberta Ingenuity Fund and the I. W. Killam Fund for post-doctoral fellowships.

References

[1] C. I. Ratcliffe, Annu. Reports NMR Spectrosc. **36,** 124 (1998).
[2] J. Bonardet, J. Fraissard, A. Gedeon, and M. Springuel-Huet, Catal. Rev. Sci. Eng. **41,** 115 (1999).
[3] A. Cherubini and A. Bifone, Prog. NMR Spectrosc. **42,** 1 (2003).
[4] C. J. Jameson, J. Chem. Phys. **116,** 8912 (2002).
[5] V. V. Terskikh, I. L. Moudrakovski, S. R. Breeze, S. Lang, C. I. Ratcliffe, J. A. Ripmeester, and A. Sayari, Langmuir **18,** 5653 (2002).
[6] C. J. Jameson and D. Stueber, J. Chem. Phys. **120,** 10200 (2004).
[7] A. K. Jameson, C. J. Jameson, and R. E. Gerald II, J. Chem. Phys. **101,** 1775 (1994).
[8] C. J. Jameson, A. K. Jameson, R. E. Gerald II, and H. M. Lim, J. Phys. Chem. **101,** 8418 (1997).
[9] T. Brotin, A. Lesage, L. Emsley, and A. Collet, J. Am. Chem. Soc. **122,** 1171 (2000).
[10] R. Grosse, B. Burmeister, B. Boddenberg, A. Gedeon, and J. Fraissard, J. Phys. Chem. **95,** 2443 (1991).
[11] R. E. Wasylishen. Probing the nanochannels of $[Co(en)_3]Cl_3$ by multinuclear NMR, X-ray diffraction and quantum chemistry calculations. Presented at the XEMAT2003 International Symposium on Xenon NMR of Materials, La Colle–sur–Loup, 29–31 May (2003).
[12] C. J. Jameson and A. K. Jameson, Mol. Phys. **20,** 957 (1971).
[13] A. D. Buckingham and P. A. Kollman, Mol. Phys. **23,** 65 (1972).
[14] C. J. Jameson, A. K. Jameson, and S. M. Cohen, Mol. Phys. **29,** 1919 (1975).
[15] C. J. Jameson, A. K. Jameson, and J. K. Hwang, J. Chem. Phys. **89,** 4074 (1988).
[16] V. Aquilanti, D. Ascenzi, D. Cappelletti, M. de Castro, and F. Pirani, J. Chem. Phys. **109,** 3898 (1998).
[17] H. Partridge and K. Faegri Jr, NASA Technical Memo No. 103918, Washington, DC (1992).
[18] D. A. Bishop and S. M. Cybulski, Chem. Phys. Lett. **211,** 255 (1993).
[19] S. Huzinaga, J. Andzelm, M. Kłobukowski, E. Radzio-Andzelm, Y. Sakai, and H. Tatewaki, *Gaussian Basis Sets for Molecular Calculations* (Elsevier, Amsterdam, 1984).
[20] M. J. Frisch, G. W. Trucks, H. B. Schlegel, *et al.*, *GAUSSIAN98, Revision A.9* (Gaussian Inc., Pittsburgh, PA, 1998).
[21] K. Wolinski, J. F. Hinton, and P. Pulay, J. Am. Chem. Soc. **112,** 8251 (1990).
[22] J. P. Jesson, in *NMR of Paramagnetic Molecules, Principles and Applications*, edited by G. N. La Mar, W. D. Horrocks Jr, and R. H. Holm (Academic Press, New York, 1973), pp. 1–52.
[23] C. J. Jameson, D. N. Sears, and A. C. de Dios, J. Chem. Phys. **118,** 2575 (2003).
[24] D. N. Sears and C. J. Jameson, J. Chem. Phys. **121,** 2151 (2004).
[25] J. Vaara and P. Pyykkö, J. Chem. Phys. **118,** 2973 (2003).
[26] M. Pecul, T. Saue, K. Ruud, and A. Rizzo, J. Chem. Phys. **121,** 3051 (2004).
[27] M. Hanni, P. Lantto, N. Runeberg, J. Jokisaari, and J. Vaara, J. Chem. Phys. **121,** 5908 (2004).

[28] P. Pyykkö, Chem. Phys. **22,** 289 (1977).
[29] P. Pyykkö and L. Wiesenfeld, Mol. Phys. **43,** 557 (1981).
[30] L. Visscher, T. Enevoldsen, T. Saue, H. J. A. Jensen, and J. Oddershede, J. Comput. Chem. **20,** 1262 (1999).
[31] J. Khandogin and T. Ziegler, J. Phys. Chem. A **104,** 113 (2000).
[32] J. Autschbach and T. Ziegler, J. Chem. Phys. **113,** 936 (2000).
[33] F. M. Chen and R. F. Snider, J. Chem. Phys. **46,** 3937 (1967).
[34] C. J. Jameson, in *Encyclopedia of Nuclear Magnetic Resonance*, edited by D. M. Grant and R. K. Harris (John Wiley, London, 1996), Vol. 4, pp. 2179–2189.